High-pressure glass-ceramics for iodine nuclear waste immobilization: Preliminary experimental results

Sami Soudani, Lucas Le Gars, Yann Morizet, Philippe Deniard, Eric Gautron, Stéphane Grolleau

HIGH-PRESSURE GLASS-CERAMICS FOR IODINE NUCLEAR WASTE IMMOBILIZATION: PRELIMINARY EXPERIMENTAL RESULTS

Sami SOUDANI[1,2], Lucas LE GARS[1,2], Yann MORIZET[1*], Philippe DENIARD[2], Eric GAUTRON[2], Stéphane GROLLEAU[2]

[1]Nantes Université, CNRS UMR6112, Laboratoire de Planétologie et Géosciences, F-44000 Nantes, France

[2]Nantes Université, CNRS, Institut des Matériaux De Nantes Jean Rouxel, IMN, F-44000 Nantes, France

*Corresponding author: Yann Morizet

Postal address:

Laboratoire de Planétologie et Géosciences (LPG), UMR-CNRS 6112, Université de Nantes.

2 rue de la Houssinière, 44322 Nantes Cedex (FRANCE)

phone: +33 (0) 2 5112 5491

fax: +33 (0) 2 5112 5268

*E-mail: yann.morizet@univ-nantes.fr

Abstract

Several matrix types have been considered for the immobilization of iodine radioisotopes from which glass-ceramics represent a serious candidate; however, I-bearing glass-ceramics are challenging owing to the iodine volatility. We have synthesised glass-ceramics from the partial crystallization of a parental glass enriched with different iodine sources (I_2 and I_2O_5) under high-pressure conditions (up to 1.5 GPa). The samples were characterized using Scanning and Transmission Electron Microscopy and X-ray Diffraction. Using standard synthesis protocol: melting, nucleation and crystal growth, we have obtained glass-ceramics showing the coexistence between I-bearing glass (<0.8 mol.% I), nepheline ($NaAlSiO_4$) and iodosodalite ($Na_8Al_6Si_6O_{24}I_2$ with up to 14 mol.% I). For several samples, we observed also the presence $NaPt_3O_4$ witnessing a chemical reaction between the container walls and the inside experimental charge. The structure of iodosodalite is entirely resolved by Rietveld refinement of the XRD pattern for I_2 experiments whereas it cannot be solved for I_2O_5 experiments suggesting a change in the iodosodalite structure probably due to the β cage filling by IO_3^- clusters instead of I^-. Our present work could represent a potential solution to tackle the problem of iodine radioisotopes immobilization.

Keywords: glass-ceramics, iodosodalite, high-pressure, nuclear waste immobilization

1. Introduction

Iodine radioisotopes are by-product of the nuclear plant industry and is of major concern in the nuclear waste immobilization [1,2]. In particular, ^{129}I is a major troublesome isotope due to its high mobility in the environment and its long half-life (15.7 My) [3-8]. Moreover, ^{129}I is shown to be the main contributor of radioactive dose at the outlet of a geological disposal site

[9,10]. For these reasons, ^{129}I represents an immediate environmental hazard and a societal risk that needs to be addressed. As a matter of fact, radioactive iodine can be incorporated into human body involving metabolic damages to the long term [11-14]. However, due to its high volatility, iodine cannot be immobilized using classical vitrification of nuclear waste bearing glass at ambient pressure [15-17]. In a recent landmark work, Riley et al. [1] reviewed this problematic and enumerated possible matrix able to efficiently immobilize iodine radioisotopes such as: crystalline phases (e.g. [18-21]), glass (e.g. [22-24]) or cement (e.g. [25]). They also pointed out that glass-ceramics could be a good candidate for the immobilization of ^{129}I with the difficulty to find a glass binder that is compatible (i.e. in equilibrium) with the I-bearing crystalline phases. From the general viewpoint, there is a growing interest in the formulation of glass-ceramics for nuclear waste immobilisation (e.g. [26-30]). Glass-ceramics have several advantages over pure crystalline or pure glass immobilization matrix: 1) higher mechanical resistance with a lower fracture propagation [31], 2) multiple barrier offering a better chemical stability [32,33] and 3) higher incorporation of nuclear waste [34,35]. Several studies [36-40] have developed experimental protocols for synthesising I-bearing glass-ceramics using iodosodalite ($Na_8Al_6Si_6O_{24}I_2$) as the I-bearing crystalline phase embedded in a sodium aluminoborosilicate glass binder. Although the developed approach involves the consolidation with a glass binder, this latter phase does not contain iodine, therefore the question remains on the thermodynamic stability through time in between the I-bearing crystalline phase and the I-free glass matrix. Although, iodosodalite crystalline phase has not been studied extensively, it appears as an appropriate crystalline phase for immobilizing radioactive iodine as 1) it incorporates a large quantity of iodine (>10 mol.% I) in its cage structure, 2) it is stable at high-temperature (up to at least 950°C, [40]), 3) it incorporates iodine under different forms, either I^- or IO_3^- [41], 4) it can be obtained using different methods (i.e. aqueous, hydrothermal and sol-gel syntheses, [40]) and

5) several studies measured the dissolution rate of iodosodalite [42,43], which showed good chemical resistance to standard leaching tests.

Obtaining a glass-ceramics requires the crystallization from a parent glass held at high temperature and cooled down to a temperature that allows nucleation and crystallization processes [44,45]. As mentioned earlier, the main difficulty with iodine is its high volatility at ambient pressure and high-temperature that prevents from iodine retention. For instance, at best the I solubility at ambient pressure in low activity waste glass compositions does not exceed 0.7 mol.% I [22]. An alternative to that problem has been developed recently by using high-pressure conditions for synthesising aluminoborosilicate glasses. The recent works [46-48] showed that the confinement pressure strongly enhances the I solubility in nuclear waste glasses. Although, this approach represents a potential solution, the chemical durability of those I-bearing matrices will remain to be determined in future studies [49].

In the present study, we demonstrate for the first time the possibility to synthesise I-bearing glass-ceramics obtained from the crystallization of a parent aluminoborosilicate glass under high-pressure conditions. The experiments were conducted with a standard thermal path involving melting-nucleation-crystallization steps, leading to the formation of a stable I-bearing silicate phase (i.e. iodosodalite) in equilibrium with a I-bearing aluminoborosilicate glass and showing no apparent open porosity. From electron microscopy and X-ray Diffraction we were able to quantify the relative crystalline phase proportions. We used different iodine sources in order to investigate the change in the iodine retention in the glass and crystals, which appears to influence the chemistry of the iodosodalite. We then discuss how iodine is incorporated qualitatively and quantitatively into our glass-ceramics; and we propose several solutions to improve the iodine assimilation into glass-ceramics.

2. Experimental and analytical methods

2.1. Starting material and high-pressure syntheses

In the present work, we studied two starting compositions noted NH and SoNH, both prepared in the SiO_2-Al_2O_3-B_2O_3-CaO-Na_2O system. In the investigated compositions, we did not add any nucleating agents. The glass compositions are reported in Table 1 and were chosen such as to represent close analogues to the low activity waste aluminoborosilicate glass compositions [50]. In between NH and SoNH, we changed the Na_2O content in order to see if the addition of Na promotes the formation of sodalite that is a Na-rich crystalline phase. The powders were prepared from a mixture of oxides for SiO_2, Al_2O_3, B_2O_3 and CaO and Na_2CO_3 for the source of Na_2O. The starting powders were grinded in an agate mortar under ethanol. The dried powders were melted in a Pt crucible at 1250°C for 2h in a box furnace and then quenched in a cold-water bath. The recovered glasses were characterized for major element concentration and glass transition temperature (T_g, see Table 1).

For the high-pressure experiments, the volatile-free glass powders were loaded into 2.5-2.9 mm Pt capsules along with I_2 or I_2O_5 powders as a source of iodine during the experiments. The solid iodine source was loaded at the bottom of the capsule prior filling with the glass powder. The Pt capsule were welded shut at both ends using arc-welder. The initial loaded I_2 or I_2O_5 range from 4.0 to 11.5 mol.% ensuring an excess iodine fluid phase during the high-pressure experiments for comparable glass compositions [46-48]. The use of different iodine sources has been shown to have a significant effect on the resulting I solubility; hence, we wanted to test if it could have an effect on the incorporation of iodine into glass-ceramics. At high temperature, the I_2O_5 dissociates into I_2 and O_2 that will impose high-oxidation state during the experiment [47]. The high-pressure experiments were conducted using piston-cylinder apparatus at 1.0 and 1.5 GPa. We used ¾ inch talc-Pyrex high-pressure assemblies in which the sample capsules were placed into MgO base ceramics. For each run, two capsules could be experimented with I_2 and I_2O_5, respectively. During the experiments, the temperature is controlled using a Eurotherm that is accurate to ±1°C and temperature is measured using a

type S thermocouple $PtRh_{10}/Pt$ located at the top of the Pt capsules. The pressure during the experiments has been controlled automatically using a Stigma© needle pump.

During the high-pressure experiments, we adopted a thermal path based on the results obtained by Differential Scanning Calorimetry (DSC) to determine T_g. The experimental protocol is described in Figure 1 and is consistent with current knowledge [45]. The main difference from existing experimental work is that high-pressure conditions are applied during the whole experiment duration. The samples held under high-pressure conditions (1.0 and 1.5 GPa) were heated up between 1200 and 1300°C for melting the experimental charges during 1h. A cooling step of 15°C/min is applied to decrease the temperature down to ~550°C that is supposed to correspond to the nucleation temperature (T_n, 50°C above T_g, [51]). The T_n duration was set to 24h; then temperature is increased to ~790°C corresponding to the crystallization temperature (T_c) as determined by DSC measurement. The T_c duration was set also to 24h then followed by the rapid isobaric quench of the high-pressure experiment (~60°C/sec) by cutting of the power. It should be emphasised that the T_n and T_c were determined from the DSC results obtained on I-free glasses prepared at ambient pressure and I-bearing pure glasses recovered from high-pressure experiments (see Table 1), therefore, those temperature conditions are only approximate considering that the obtained T_n and T_c are not determined in-situ under high-pressure conditions. Moreover, in our experiments, the temperature is measured by the thermocouple at the top of the capsules and temperature gradient is occurring on the capsule length (~50°C over ~10 mm capsule length, [52]). After the experiment, most of the recovered glass-ceramics are covered with a I_2 black residue that is removed in ethanol bath. Although we did not quantify the iodine coating, it suggests that an excess fluid phase was always present during the experiments. The glass-ceramics were scrutinized using optical microscope to confirm the presence of both glass and crystalline materials.

In addition, ambient pressure crystalline iodosodalite ($Na_8Al_6Si_6O_{24}I_2$) has been synthesised using the protocol described in Warner et al. [53]. We used zeolite A ($Na_{12}Al_{12}Si_{12}O_{48}$) and NaI as precursors, mixed in 1:16 molar proportions. The powder has been homogenized in a ball milling at 400 rpm for 6h under ethanol, dried overnight at 80°C. The reaction is finalized by heating the powder at 900°C for 8h in box furnace. The obtained iodosodalite powder serves as a fingerprint for the characterization of the high-pressure glass-ceramics with X-ray Diffraction.

2.2. Characterization methods

Several chips were mounted in epoxy plugs, polished under glycerol to avoid crystalline phase reaction and coated with carbon for Scanning Electron Microscopy (SEM) analyses. We used two types of SEM (IMN Jean Rouxel): a JEOL JSM 5800LV equipped with an Energy Dispersive Spectrometer (EDS) for the major element (including iodine) quantitative analyses, a JEOL JSM 7600F for obtaining high-resolution imaging of the crystalline phases as well as a mapping of the elemental concentration. For the JEOL JSM 5800LV SEM EDS analyses, the analytical conditions were 15 kV for voltage and 0.5 nA for current. We conducted the acquisitions on a 10 µm spot size to avoid Na loss under the electron beam. Five scans of 1 min were collected on each sample at different location on the glass chip. For the JEOL JSM 7600LV SEM mapping, the analytical conditions were 10 kV for voltage and 0.5 nA for current. The high-resolution mapping was acquired using backscattered electron. The dot mapping was acquired on 800 x 600 pixels (24 x 18 µm) at a dwell time of 15 µs per pixel and corresponding to a 20 min data collection. The element quantification was conducted using the following internal standard on the SEM EDS: corundum for Al_2O_3, wollastonite for SiO_2 and CaO, NaCl for Na_2O, RbI for I. Due to the low boron mass, we did not analyze B_2O_3 that is not correctly quantified using SEM EDS analyses. The mol.% B_2O_3 reported in Table 1 corresponds to the shortfall obtained from SEM EDS analyses. The error

calculated on the determined mol.% major element oxides in both the I-free and I-bearing glasses and the matrix of the glass-ceramics is on the order of ±0.5 mol.% based on the standard deviation of replicated measurements (Table 1). We also could analyze the chemical compositions of iodosodalite crystals. The I content of the iodosodalite crystals is provided in Table 2; however, it should be pointed out that, owing to the small size of this crystalline phases, the error on the reported mol.% I in Table 2 is probably large. Even though the iodosodalite mol.% I is based on multiple measurements (at least five different crystals), we cannot exclude to the measurement a potential contribution from the surrounding matrix (glass + nepheline) with low I content.

We also conducted Scanning/Transmission Electron Microscopy (S/TEM) at 80 kV on a Cs probe corrected Themis Z G3 (Thermo Fisher Scientific) using the High Angle annular Dark Field (HAADF) detector (with 33-197° collection angle range) and the 4-SDD detectors (Super-X system) for EDS analysis. Samples were previously prepared by dispersing the grinded powder in ethanol and depositing a drop of this solution on a holey-carbon-coated copper grid.

We performed the Differential Scanning Calorimetry (DSC) on two different apparatus to determine T_g and T_c: a Q20 TA Instruments and a Sensys Evo SETARAM, at IMN Jean Rouxel. The DSC was calibrated against the melting enthalpy of lead. The blank was performed using an empty reference alumina crucible. The samples were crushed and ~20 mg of glass sample was analysed each time. The heating profile was a heating ramp from ambient temperature to 850°C at 5°C/min. The furnace was purged with inert gas (N_2) with a flow of 20 mL/min during the heating cycle. The T_g value was determined using the variation of the measured heat flow (mW) and the two tangents method using the implemented software procedure in Universal Analysis 2000© for the Q20 TA Instruments and Calisto© software

for the Sensys Evo SETARAM. The T_c value is extracted from the exothermic peak on the DSC curves.

For all the glass ceramic samples, the X-ray Diffraction (XRD) patterns have been obtained using and INEL XRG3500 operating at 40 kV and 20 mA at IMN Jean Rouxel allowing small sample size using capillary and Debye-Scherrer geometry. The simultaneous acquisitions were performed on a 120° angle with a step of 0.03° in 2θ. We used the Cu Kα1 wavelength at 1.5406 Å monochromated using quartz crystal. Sample acquisitions were conducted in 0.2 and 0.3 mm in diameter capillary. The acquisition duration was between 6 and 24h with a 2s time per step. As we obtained a large quantity of iodosodalite synthesised at 1 bar pressure (see Table 2, Iodo 1bar), the XRD acquisition was performed on a Bruker D8 II with a Bragg-Brentano geometry equipped with a Cu Kα1 wavelength at 1.5406 Å and monochromated using germanium (111). The obtained diffractograms were pre-treated using DIFFRAC.EVA© software and the PDF-2 database to find the association of crystalline phases present in our material. We then conducted the Rietveld refinement [54] with JANA2020© software [55] for determining the crystallographic structure of the mineral phases and their proportions (see Table 2).

3. Results and discussion

3.1. Thermal analyses as a function of experimental conditions and iodine content

Typical DSC curves are shown in Figure 2 and are obtained for 1) ambient pressure I-free NH and SoNH glasses and 2) I-bearing glasses synthesised at 1 GPa and 1300°C equilibrated with either I_2 or I_2O_5 fluid phase, SoNH_I_2-0 and SoNH_I_2O_5-0, respectively. The I content in the glasses is reported in Table 1: 0.6 mol.% and 1.2 mol.% for SoNH_I_2-0 and SoNH_I_2O_5-0, respectively. The present result can be compared to the results obtained in Jolivet et al. [46] for low activity waste glasses synthesised at identical pressure (~1.5 mol.% I at 1.5 GPa). The

obtained T_g is ranging from 510 to 531°C determined from the double tangent method. We observe that the T_g is only weakly affected by either the high-pressure conditions or the presence of dissolved iodine in agreement with the results shown in Jolivet et al. [56] suggesting that increasing I dissolution slightly decreases T_g values. It is assumed that T_n value is close to T_g value (~+50°C). In our case, the curves shown in Figure 2 suggest a T_n value close to 560 and 590°C for SoNH_1b and NH_1b, respectively. As the crystallization corresponds to an exothermic phenomenon, the T_c is represented by the positive peak observed in Figure 2 and is estimated to be close to 790°C. Those derived T_n and T_c values were used in our experimental protocol shown in Figure 1 for synthesising the glass-ceramics. However, as emphasised previously, the adopted protocol constitutes a first approach and further improvements in the temperature path and constraints are required during the high-pressure experiments. This aspect will be further discussed in the following sections.

3.2. Iodine incorporation into glass and glass-ceramics at high-pressure

We present in Figure 3 two typical SEM element mapping images obtained on a JEOL JSM 7600LV for NH_I_2-2 and NH_I_2O_5-2 synthesised at 1.0 GPa with T_n = 594°C and T_c = 813°C both temperature for 24h run duration, respectively. The images in Figure 3 show the coexistence between a glass matrix in grey and disseminated euhedral crystals in bright. It should also be emphasised that there is no apparent porosity in the obtained samples that is compulsory for the glass-ceramics durability [45]. The change in brightness in between the crystals and glass suggests that the observed crystalline phases are enriched with respect to heavier elements (i.e. iodine) as compared to the matrix. In Figure 3, we have reported the elemental distribution for Si, Al, I and Pt; however, we also obtained the Ca and Na elemental mapping for the same samples but not provided here for clarity. For both samples, we observe that Al is more concentrated in the observable crystalline phase than in glass matrix; and I is much more concentrated in the observed bright euhedral crystals than in the surrounding

252 matrix. The I-bearing crystalline phase is interpreted as iodosodalite (Is.) and also confirmed
253 by XRD measurements. Those results are consistent with our knowledge of the iodosodalite
254 chemical composition that has high Al_2O_3 content (20 mol.%) and high I content (13.3 mol.%
255 I) that are contrasting with the glass Al_2O_3 and I contents: ~10 mol.% and <1 mol.%,
256 respectively. We also observe from the Al and I mapping images in NH_I_2O_5-2, a crystalline
257 phase that is enriched with respect to Al and that does not contain I and is interpreted as
258 nepheline crystal (Neph.). Interestingly, this crystal is not observed in the backscattered image
259 suggesting that the contrast in elemental mass in between the glass matrix and the nepheline
260 crystals is low. This represents a major problem as the quantitative analysis of the glass-
261 ceramics phase proportions (i.e. glass, nepheline and iodosodalite) is not possible from image
262 analysis. Consequently, in Table 1, we refer to the matrix composition as an association
263 between nepheline and glass instead of the glass composition. As shown in Table 2, the
264 nepheline has been identified in several samples, regardless of the initial iodine source. The
265 presence of nepheline is a negative aspect for the formulation of a reliable glass-ceramics
266 immobilizing iodine radioisotopes. Previous studies showed that the nepheline crystallization
267 is particularly detrimental for the durability of the nuclear waste form [29,57,58]. The
268 presence of nepheline could have several explanations. It is possible that local iodine
269 depletion prevents from the crystallization of additional iodosodalite crystals. Although the
270 experiments were conducted above T_g and the system is supposed to behave like a liquid (i.e.
271 instantaneous change in the physical properties; [59]), it might be possible that the I diffusion
272 is not fast enough and the crystallization of nepheline occurs well before an equilibration of
273 the I content could occur. Another explanation is that the adopted experimental conditions,
274 especially pressure conditions (1.0 and 1.5 GPa), are, at some stage, outside the
275 thermodynamic stability field of iodosodalite and nepheline becomes the more stable
276 crystalline phase. We also identified the presence of a Pt-rich phase that appears very bright in

277 the backscattered image of the NH_I_2O_5-2 sample. The XRD analysis revealed that it
278 corresponds to $NaPt_3O_4$ suggesting that there is a chemical reaction between the Pt capsule
279 walls and the sample charge during the experiment.

280 The SEM EDS results are given in Table 1 for 1) the pure glass either I-free or I-bearing and
281 2) the matrix composition of the glass-ceramics and considered to be an association between a
282 I-bearing glass and I-free nepheline crystalline phase. The error bars on the I content based on
283 the standard deviation of the replicated measurements is on the order of ±0.2 mol.%. For pure
284 glass samples, we observe that I content in the glass is higher in the case I_2O_5 is the I source
285 as compared to I_2. For instance, we measured 0.7 and 1.5 mol.% I in NH_I_2-0 and NH_I_2O_5-0
286 glass loaded with I_2 and I_2O_5, respectively. The same applies to the SoNH glass composition
287 in which we measured 0.6 and 1.2 mol.% I for SoNH_I_2-0 and SoNH_I_2O_5-0, respectively.
288 The higher I content measured in glasses with initial I_2O_5 source is consistent with the recent
289 results from Morizet et al. [47] suggesting that I solubility is enhanced in that case owing to
290 the stabilization of IO_3^- molecular groups within the glass structure. In the present work for I_2
291 experiments, the measured I solubility (0.6 and 0.7 mol.% I for SoNH_I_2-0 and NH_I_2-0,
292 respectively) is significantly lower than the one reported in Jolivet et al. [46] (~1.5 mol.% I)
293 for identical intensive conditions. Despite the higher Na_2O content in SoNH (~24 mol.%)
294 compared to NH (19 mol.%) the measured mol.% I is lower in SoNH. Such result was not
295 expected considering that recent studies have shown that I solubility is positively affected by
296 the alkali concentration [47,60]. There is also a difference in the run duration in between both
297 glass compositions: 3h for NH and 10h for SoNH. We wanted to check if changing the run
298 duration could induce a change in the I solubility and by extension could impact the I
299 dissolution for glass-ceramics, which are equilibrated with longer run duration. As observed
300 in Table 1, we suggest that there is no change in the I solubility with increasing run duration.

301 This implies that the equilibrium between the I-rich fluid phase and the melt at high
302 temperature is reached early in the experiment.

303 Globally, the I content measured in the matrix of the glass-ceramics appears lower than the
304 pure equivalent glass. This is especially true for the NH glass ceramic samples in which the I
305 content does not exceed 0.5 mol.% I (see Table 1). This observation is less obvious for SoNH
306 glass ceramic samples. For instance, 0.8 mol.% I has been determined the glass matrix for the
307 SoNH_I_2-1 whereas 0.6 mol.% I has been measured in the pure glass SoNH_I_2-0 in
308 equilibrium with I_2 fluid phase and for identical pressure conditions (1.0 GPa). The decrease
309 of the I content in the glass matrix is more pronounced for the samples equilibrated with I_2O_5
310 fluid phase: 0.7 mol.% I is measured in the SoNH_I_2O_5-2 glass ceramic whereas 1.2 mol.% I
311 is determined for the equivalent pure glass SoNH_I_2O_5-0. Moreover, in between those
312 samples, there is a difference in pressure synthesis: 1.5 GPa for the SoNH_I_2O_5-2 glass
313 ceramic and 1.0 GPa for the SoNH_I_2O_5-0 glass; that would induce higher I dissolution in the
314 glass-ceramics than in glass as pressure is thought to have a positive effect on the I dissolution
315 [46,48,61,62]. Nonetheless, the decrease in I content in the matrix for the glass ceramic
316 samples is explained by the fact that the crystallization of I-bearing crystalline phases depletes
317 the bulk composition with respect to iodine. Another explanation is the presence of nepheline
318 crystals that are I-free and are not observed using SEM. Therefore, the analysis of the matrix
319 glass-ceramics composition will result in an even lower I content. The presence of
320 iodosodalite crystals that are Na-rich crystalline phases also points towards the depletion of
321 Na_2O in the chemical composition of the glass ceramic matrices. As can be seen in Table 1,
322 the matrix compositions are systematically depleted in Na_2O (~21.0 mol.% Na_2O) for SoNH
323 glass-ceramics as compared to the pristine SoNH glass (~24.0 mol.% Na_2O). As inferred
324 earlier, the decrease in Na_2O content of the glass matrix does not favour I dissolution

[24,48,60]; however, Na_2O decrease will induce an increase in the degree of polymerization of the glass matrix network and therefore potentially increase the glass durability [29,48,63].

We have pushed further the analysis of the glass-ceramics by conducting S/TEM mapping at nm scale as shown in Figure 4 on NH-I_2-2. We found sample chips exhibiting different compositions that can be attributed to the identified coexisting phases: nepheline, iodosodalite and glass. The nepheline and iodosodalite are Ca-free whereas the glass is Ca-bearing. A small amount of Ca (~1 at.%) is present in the area assigned to nepheline. This could be explained by the superposition of this phase with the glass. The iodosodalite has the following composition (with an associated error of ±20% in relative): 25.0 Na_2O, 19.2 Al_2O_3, 44.5 SiO_2 and 11.3 mol.% I; that is very close to the theoretical composition: 26.7 Na_2O, 20.0 Al_2O_3, 40.0 SiO_2 and 13.3 mol.% I. The measured glass composition is: 16.3 Na_2O, 12.7 Al_2O_3, 61.1 SiO_2 and 10.0 mol.% CaO; the I content of the glass could not be determined due to the overlapping between the I Lα and Ca Kβ lines and the low I concentration in glass. The derived glass composition is strongly enriched in SiO_2, depleted in Na_2O and slightly enriched in CaO as compared to the initial starting glass composition (see Table 1). The crystallization of iodosodalite and nepheline will decrease significantly the Na_2O of the matrix considering that those phases are Na-rich.

Although the presented results provide a proof-of-concept, substantial improvements in the syntheses method are required in order to 1) avoid the crystallization of nepheline crystals during the high-pressure synthesis that is a low durability phase, 2) increase the proportion of iodosodalite crystals that are known to incorporate large amount of I under either I^- or IO_3^- into the β-cage and 3) increase the size of the iodosodalite crystals for better characterization. Nevertheless, we propose the first attempt for glass-ceramics obtained from heterogeneous nucleation from the parental glass under high-pressure conditions showing the coexistence between an I-bearing glass matrix and an I-bearing crystalline phase.

3.3. Iodosodalite crystal-chemistry

We focused on the crystal-chemistry of the obtained iodosodalite using XRD and Rietveld refinement. In Figure 5, we show one diffractogram obtained for NH_I_2-2 equilibrated at 1.0 GPa. Additional diffractograms are also provided in the Suppl. Mat.. The identified diffraction peaks for $NaPt_3O_4$, nepheline and iodosodalite are indicated. We observe a strong non-linear background that is assigned to the contribution of the glass amorphous phase. Unfortunately, without calibration compound, we are not able to determine the proportion of the amorphous glass in the glass ceramic samples. The peaks for $NaPt_3O_4$ are strong in intensity due to the high cubic symmetry (space group O_h^3 – P*m*-3*n*, [64]). We give in Table 2 the lattice parameters derived from Rietveld refinement for crystalline phases, the associated space group and the wRp parameter. This latter parameter represents the reliability parameter with respect to the structure refinement. We also reported the I content in iodosodalite as measured from SEM EDS and based on at least 5 measurements on different crystals. It should be emphasised that, for iodosodalite structure, the Rietveld refinement has been adequately conducted for I_2 samples whereas it is only partially resolved for I_2O_5 samples (see Table 2).

The nepheline structure shows a hexagonal lattice with a space group $P6_3$. We calculated an average value for the cell parameters and we obtained 9.940±0.012 and 8.320±0.013 Å for a and c, respectively. The small standard deviation in the cell parameters suggest that the structure of nepheline is roughly constant in between the glass ceramic samples. The nepheline structure has been investigated a long ago [65-67]. Buerger et al. [65] reported 10.05 and 8.38 Å for the lattice parameter values, which is significantly higher than the ones we obtain. We explain the lower a and c values in our nepheline by the high-pressure synthesis conditions. It is currently known that increasing pressure conditions induces a decrease in the lattice volume and parameters. Recent work by Diego Gatta and Angel [68]

showed that increasing pressure decreases the cell parameters for nepheline (i.e. K- and Na-bearing natural nepheline). In their work, the a and c parameters change from 9.9995 and 8.3766 Å to 9.8499 and 8.2838 Å between ambient and 2.0 GPa pressure.

To conduct the Rietveld refinement for iodosodalite structure, we used the CIF reference 1534899 from the Crystallographic Open Database and reported in Beagley et al. [69]. The obtained lattice parameter is on the order of 9 Å with a cubic space group I-43*m* that is consistent with previous results [41,70,71]. For instance, Chong et al. [71] gives a cell parameter at 9.009 Å for iodosodalite crystals obtained by hydrothermal synthesis. Systematically, the derived cell parameter for the high-pressure iodosodalite is lower (on average 9.007±0.004 Å on the reported structures in Table 2) than the one obtained for the ambient pressure iodosodalite (9.0295 Å). As for nepheline, we suspect that the high-pressure conditions explain the decrease in the lattice parameter for iodosodalite.

We mentioned earlier that the Rietveld refinement was incomplete for I_2O_5 samples as opposed to the I_2 samples in which the resolution of the iodosodalite crystalline structure is complete using standard crystalline model for the structure of iodosodalite. We suspect that this reference is not adapted for the iodosodalite crystalline structure obtained in the I_2O_5 glass ceramic samples. One possible reason is that the iodosodalite crystals obtained have β cages occupied by IO_3^- instead of I^- clusters or a combination of both species. Currently, we are unable to confirm the difference in cage occupancy.

3.4. Estimate of the iodine budget in glass-ceramics

In the absence of reliable quantification of the glass phase in the glass-ceramics, it is not possible to constrain the I content in the glass-ceramics. It is even more complicated by the fact that the concentration of nepheline crystals cannot be obtained from the SEM owing to the low contrast difference in between the glass phase and the nepheline crystalline phase (see

399 Figure 3). Currently, the only information that can be obtained is the relative proportion of the
400 different crystalline phases. We have reported the proportion of the different phases in Figure
401 6 (data are provided in Table 2) as determined from XRD analyses. The wt.% for each
402 crystalline phases is represented for each glass ceramic sample and categorized as a function
403 of the initial iodine source (either I_2 or I_2O_5). It should be pointed out that, considering the
404 incomplete Rietveld refinement for I_2O_5 samples, the crystalline phase proportions are subject
405 to large errors. For the I_2-bearing glass-ceramics, we observe that the proportion of nepheline
406 seems more important in the SoNH samples (>70 wt.%) than in the NH samples (<50 wt.%),
407 for identical synthesis conditions (1.0 GPa pressure for NH_I_2-1 and -2 and SoNH_I_2-1).
408 Conversely, it corresponds to an increased proportion of iodosodalite in NH than SoNH
409 samples. It suggests that increasing the Na_2O in the starting composition (i.e. SoNH) does not
410 favour the crystallization of iodosodalite as initially thought. Instead, the higher Al/Na ratio in
411 the NH compared to SoNH is likely to enhance the stability of iodosodalite that is Al-rich.
412 Although it remains to be confirmed with additional experiments, it seems that the nepheline
413 proportion decreases and the proportion of iodosodalite increases in I_2O_5-bearing samples in
414 comparison to the I_2-bearing samples. The proportion of $NaPt_3O_4$ appears very low (<2 wt.%)
415 or even zero in the I_2-bearing samples. On the other hand, even with large associated errors
416 the $NaPt_3O_4$ is unambiguously identified in I_2O_5-bearing samples from XRD (see Figure 6). It
417 suggests that there is a chemical reaction in between the Pt walls of the sample container with
418 the inside fluid phase (I_2 and O_2) and the sodium of the matrix. This reaction has been clearly
419 identified for SoNH_I_2-0 and SoNH_I_2O_5-0 glasses and is described in the Suppl. Mat.. The
420 identified mass proportion of $NaPt_3O_4$ in the different samples (see Table 2) does not affect
421 the glass composition with respect to the Na incorporation. For instance, the 16 wt.% $NaPt_3O_4$
422 in NH_I_2O_5-1 corresponds to 0.5 wt.% Na incorporated into the $NaPt_3O_4$, which can be
423 considered as negligible with regards to the total Na2O content within the glass matrix (~20

wt.%) and is likely to have a minor influence on the crystallization of the Na-bearing crystalline phases (i.e. iodosodalite and nepheline).

Further experiments are required in order to improve the iodine incorporation. For instance, the percentage of I-bearing crystalline phase needs to be increased and the presence of nepheline should be avoided. We suggest that the NH composition is probably more adequate than the SoNH in the formulation of a glass ceramic for immobilizing ^{129}I nuclear waste due to the higher Al/Na ratio in NH composition. We suggested that the presence of nepheline could be due to the intensive conditions that are close to be outside the pressure and temperature stability field of iodosodalite. For instance, previous works on Cl-bearing sodalite [72,73] showed that the stability field of sodalite is located at low pressure and sodalite becomes unstable above 0.8 GPa. As a result, we should consider performing experiments at lower pressure (i.e. <0.5 GPa) that is likely to improve the stability of the iodosodalite phase. Moreover, lowering the pressure condition is also beneficial as those pressure conditions can be achieved industrially [1].

4. Summary

In the present work, we demonstrate the possibility to synthesise glass-ceramics that are able to incorporate iodine content in both the glass and the crystalline phases with the objective to propose a formulation for the immobilisation of ^{129}I radioisotopes. The glass-ceramics were obtained from the nucleation and crystallization of a parent aluminoborosilicate glass under high-pressure conditions (1.0 and 1.5 GPa) and using different iodine source: I_2 and I_2O_5.

The glass ceramic analyses shows the coexistence between a glass matrix containing iodine (up to 0.8 mol.%) and various crystalline phases. The crystalline phases are iodosodalite, nepheline and $NaPt_3O_4$. This latter phase is mostly present in the glass-ceramics equilibrated with I_2O_5 source. The presence of nepheline is detrimental for the durability of the glass-

ceramics and further improvements in the experimental protocol are required. Experiments at lower pressure might be of interest as we could avoid the crystallization of nepheline. For now, due to the small crystal size (<10 µm) we are only able to determine the local environment of iodine into the iodosodalite if it is filled with I^- species. When IO_3^- or both species are present inside the cage (i.e. solid solution of iodate and iodide sodalite), the DRX appears limited due to the lack of structural model in that case. The obtained results are encouraging and request further experimental work for formulating a glass-ceramics able to incorporate large iodine quantities in both the glass matrix and iodosodalite crystalline phase conferring mechanical durability, chemical durability through the double barrier, and higher nuclear waste load advantages.

Acknowledgements: The authors are grateful to the Agence Nationale de la Recherche and Région Pays de la Loire, which financed the current work through the ANR project ‘‘Iodine-CLEAN-UP’’ (ANR-20-CE08-0018) and the Pari Scientifique ‘‘CIPress’’. The authors thank the Laboratoire de Planétologie et Géosciences, the Institut des Matériaux de Nantes Jean Rouxel, Nantes Université and the CNRS for providing access to the analytical facilities. The authors thank Nicolas Stephant for its support on the SEM/EDS analytical platform.

References

[1] B.J. Riley, J.D. Vienna, D.M. Strachan, J.S. McCloy, J.L.Jr. Jerden, Materials and processes for the effective capture and immobilization of radioiodine: a review, J. Nuc. Mat. 470 (2016) 307–26.

[2] R.C. Moore, C.I. Pearce, J.W. Morad, et al., Iodine immobilization by materials through sorption and redox-driven processes: a literature review, Sci. Total Environ. 716 (2020) 132820.

[3] A. Aldahan, V. Alfimov, G. Possnert G., ^{129}I anthropogenic budget: major sources and sinks, Appl. Geochem. 22 (2007) 606-618.

[4] E. Englund, A. Aldahan, X.L. Hou, et al., Iodine (^{129}I and ^{127}I) in aerosols from northern Europe, Nucl. Instrum. Method Phys. Res. B 268 (2010) 1139–1141.

[5] R. Michel, A. Daraoui, M. Gorny, et al., Iodine-129 and iodine-127 in European seawaters and in precipitation from Northern Germany, Sci. Total Environ. 419 (2012) 151–169.

[6] P. He, X. Hou, A. Aldahan, G. Possnert, Radioactive ^{129}I in surface water of the Celtic Sea, J. Radioanal. Nucl. Chem. 299 (2014) 249-253.

[7] X. Chen, M. Gong, P. Yi, et al., Distribution of ^{129}I in terrestrial surface water environments, Nucl. Instrum. Methods Phys. Res. B 361 (2015) 604–608.

[8] Y. Fan, X. Hou, W. Zhou, G. Liu, ^{129}I record of nuclear activities in marine sediment core from Jiaozhou Bay in China, J. Environ. Radioact. 154 (2016) 15–24.

[9] O. Méplan, A. Nuttin, La gestion des déchets nucléaires, Images de la Physique (2006) 9-17.

[10] H.E. Shim, J.E. Yang, S.-W. Jeong, C.H. Lee, L. Song, S. Mushtaq, D.S. Choi, Y.J. Choi, J. Jeon, Silver nanomaterial-immobilized desalination systems for efficient removal of radioactive iodine species in water, Nanomat. 8 (2018) 660.

[11] C.M. Grossman, W.E. Morton, R.H. Nussbaum, Hypothyroidism and spontaneous abortions among Hanford, Washington, downwinders, Arch. Environ. Health 51 (1996) 175–176.

493 [12] C.M. Grossman, R.H. Nussbaum, F.D. Nussbaum, Thyrotoxicosis among Hanford,
494 Washington, Downwinders: a communitybased health survey, Arch. Environ. Health 57
495 (2002) 9–15.

496 [13] C.M. Grossman, R.H. Nussbaum, F.D. Nussbaum, Cancers among residents downwind
497 of the Hanford, Washington, plutonium production site, Arch. Environ. Health 58 (2003)
498 267–274.

499 [14] J.R. Goldsmith, C.M. Grossman, W.E. Morton, R.H. Nussbaum, E.A. Kordysh, M.R.
500 Quastel, R.B. Sobel, F.D. Nussbaum, Juvenile hypothyroidism among two populations
501 exposed to radioiodine, Environ. Health Perspect. 107 (1999) 303–308.

502 [15] M.J. Plodinec, Borosilicate glasses for nuclear waste immobilisation, Glass Technology
503 41 (2000) 186–192.

504 [16] P. Hmra, Retention of Halogens in Waste Glass, U.S. department of energy Pacific
505 Northwest National Laboratory (2010) 19361.

506 [17] B.K. Maji, H. Jena, R. Asuvathraman, Electrical conductivity and glass transition
507 temperature (Tg) measurements on some selected glasses used for nuclear waste
508 immobilization, J. Non-Cryst. Solids 434 (2016) 102–107.

509 [18] L. Campayo, A. Grandjean, A. Coulon, et al., Incorporation of iodates into
510 hydroxyapatites: a new approach for the confinement of radioactive iodine, J. Mater. Chem.
511 21 (2011) 17609.

512 [19] L. Campayo, F. Audubert, J.E. Lartigue, E. Courtois-Manara, S.L. Gallet, F. Bernard, T.
513 Lemesle, F.O. Mear, L. Montagne, A. Coulon, et al., French studies on the development of
514 potential conditioning matrices for iodine 129, Mater. Res. Soc. Symp. Proc. 1744 (2015) 15-
515 20.

[20] A. Coulon, D. Laurencin, A. Grandjean, C. Cau Dit Coumes, S. Rossignol, L. Campayo, Immobilization of iodine into a hydroxyapatite structure prepared by cementation, J. Mat. Chem. A 2 (2014) 20923–20932.

[21] K. Yang, W. Zhu, S. Scott, Y. Wang, J. Wang, B.J. Riley, et al., Immobilization of cesium and iodine into $Cs_3Bi_2I_9$ perovskite-silica composites and core-shell waste forms with high waste loadings and chemical durability, J. Haz. Mat. 401 (2020) 123279.

[22] B.J. Riley, M.J. Schweiger, D.-S. Kim, W.W. Lukens, B.D. Williams, C. Iovin, et al.? Iodine solubility in a low-activity waste borosilicate glass at 1000°C. J. Nuc. Mat. 452 (2014) 178–88.

[23] I.S. Muller, D.A. McKeown, I.L. Pegg, Structural behavior of Tc and I ions in nuclear waste glass, Proc. Mater. Sci. 7 (2014) 53–9.

[24] D.A. McKeown, I.S. Muller, I.L. Pegg, Iodine valence and local environments in borosilicate waste glasses using X-ray absorption spectroscopy, J. Nuc. Mat. 456 (2015) 182–191.

[25] R.D. Scheele, C.F. Wend, W.C. Buchmiller, A.E. Kozelisky, R.L. Sell, Preliminary evaluation of spent silver mordenite disposal forms resulting from gaseous radioiodine control at Hanford's waste treatment plant, Pacific NorthWest Division (2002) 3225.

[26] D. Caurant, P. Loiseau, O. Majerus, V. Aubin-Chevaldonnet, I. Bardez, A. Quintas, Glasses, glass-ceramics and ceramics for immobilization of highly radioactive nuclear wastes. Nova Science Publishers, Inc., New York, 2009.

[27] I.W. Donald, Waste immobilization in glass and ceramic based hosts: Radioactive, toxic, and hazardous wastes. Wiley, Chichester, West Sussex, 2010.

538 [28] J. McCloy, A. Goel, Glass-ceramics for nuclear-waste immobilization, MRS Bull. 42
539 (2017) 233240.

540 [29] D. Caurant, O. Majérus, Glasses and glass-ceramics for nuclear waste immobilization.
541 Reference Module in Materials Science and Materials Engineering. Elsevier, Oxford, 2021.

542 [30] J. McCloy, S. Schuller, Vitrification of wastes: from unwanted to controlled
543 crystallization, a review, Comptes Rendus Géoscience – Sciences de la planète 354 (2022)
544 121-160.

545 [31] W. Höland and G. Beall. Glass-ceramics technology. The American Ceramic Society,
546 2002.

547 [32] R.C. Ewing, W. Lutze, High-level nuclear waste immobilization with ceramics, Ceram.
548 Int. 17 (1991) 287293.

549 [33] P. Loiseau, D. Caurant, N. Baffier, L. Mazerolles, C. Fillet, Glass–ceramic nuclear waste
550 forms obtained from SiO_2–Al_2O_3–CaO–ZrO_2–TiO_2 glasses containing lanthanides (Ce, Nd,
551 Eu, Gd, Yb) and actinides (Th): study of internal crystallization, J. Nuc. Mat. 335 (2004) 14-
552 32.

553 [34] I.W. Donald, B.L. Metcalfe, R.N.J. Taylor, The immobilization of high level radioactive
554 wastes using ceramics and glasses, J. Mater. Sci. 32 (1997) 5851–5887.

555 [35] W.E. Lee, M.I. Ojovan, M.C. Stennett, N.C. Hyatt, Immobilisation of radioactive waste
556 in glasses, glass composite materials and ceramics, Adv. Appl. Ceram. 105 (2006) 3–12.

557 [36] S. Chong, J.A. Peterson, B.J. Riley, et al., Glass-bonded iodosodalite waste form for
558 immobilization of ^{129}I, J. Nuc. Mat. 504 (2018) 109–121.

559 [37] S. Chong, B.J. Riley, R.M. Asmussen, et al., Iodosodalite synthesis with hot isostatic
560 pressing of precursors produced from aqueous and hydrothermal processes, J. Nuc. Mat. 538
561 (2020) 152222.

562 [38] H. An, S. Kweon, S. Park, et al., Immobilization of radioiodine via an interzeolite
563 transformation to iodosodalite, Nanomat. 10 (2020) 2157.

564 [39] M. Hassan, S. Venkatesan, H.J. Ryu, Nonvolatile immobilization of iodine by the
565 coldsintering of iodosodalite, J. Hazard. Mat. 386 (2020) 121646.

566 [40] J.O. Kroll, B.J. Riley, J. McCloy, J.A. Peterson, Sol–gel synthesis of iodosodalite
567 precursors and subsequent consolidation with a glass binder made from oxides and sol–gel
568 routes. J. Sol-Gel Sci. Tech. 96 (2020) 564-575.

569 [41] J.-C. Buhl, The properties of salt-filled sodalities. Part 4; Synthesis and heterogeneous
570 reactions of iodate-enchlathrated sodalite $Na_8[AlSiO_4]_6(IO_3)_{2-x}(OH.H_2O)_x$; $0.7 < x < 1.3$,
571 Thermochim Acta. 286 (1996) 251-262.

572 [42] E. Maddrell, A. Gandy, M. Stennett, The durability of iodide sodalite. J. Nuc. Mat. 449
573 (2014) 168-172.

574 [43] Y. Feng, G. Wei, Y. Liu, W. Han, Y. Chen, et al., Crystallization behavior of boron in
575 low-temperature immobilization of iodine waste. J. Solid State Chem. 305 (2022) 122698.

576 [44] M. Allix, L. Cormier, Crystallization and glass-ceramics, In: Musgraves JD, Hu J, Calvez
577 L, editors. Springer Handbook of Glass. Springer Handbooks Cham, 2019; p. 113-167.

578 [45] J. Deubener, M. Allix, M.J. Davis, A. Duran, T. Höche, T. Honma, T. Komatsu, S.
579 Krüger, I. Mitra, R. Müller, S. Nakane, M.J. Pascual, J.W.P. Schmelzer, E.D. Zanotto, S.
580 Zhou, Updated definition of glass-ceramics. J. Non-Cryst. Solids 501 (2018) 3–10.

[46] V. Jolivet, Y. Morizet, M. Paris, T. Suzuki-Muresan, High pressure experimental study on iodine solution mechanisms in nuclear waste glasses, J. Nuc. Mat. 533 (2020) 152112.

[47] Y. Morizet, J. Hamon, C. La, et al., Immobilization of ^{129}I in nuclear waste glass matrixes synthesized under high-pressure conditions: an experimental study, J. Mater. Chem. A 9 (2021) 23902–23915.

[48] Y. Morizet, M. Paris, J. Hamon, C. La, S. Grolleau, T. Suzuki-Muresan, Predicting iodine solubility at high pressure in borosilicate nuclear waste glasses using optical basicity: an experimental study, J. Mat. Sci. 57 (2022) 16600–16618.

[49] H. Zhang, T. Suzuki-Muresan, Y. Morizet, S. Gin, A. Abdelouas, Investigation on boron and iodine behavior during nuclear glass vapor hydration, Nature Mat. Degrad. 5 (2021) 1-9.

[50] G.F. Piepel, S.K. Cooley, J.D. Vienna, J.V. Crum, Experimental design for Hanford low-activity waste glasses with high waste loading, US Department of Energy, Pacific Northwest National Laboratory (2015) 24391.

[51] H. Li, L. Wu, D. Xu, X. Wang, Y. Teng, Y. Li, Structure and chemical durability of barium borosilicate glass-ceramics containing zirconolite and titanite crystalline phases, J. Nuc. Mat. 466 (2015) 484-490.

[52] Y. Morizet, R.A. Brooker, S.C. Kohn, CO_2 in haplo-phonolite melt: Solubility, speciation and carbonate complexation, Geochim. Cosmochim. Acta 66 (2002) 1809-1820.

[53] T.E. Warner, J. Hutzen Andersen, The effects of sulfur intercalation on the optical properties of artificial ‘hackmanite’, $Na_8[Al_6Si_6O_{24}]Cl_{1.8}S_{0.1}$; ‘sulfosodalite’, $Na_8[Al_6Si_6O_{24}]S$; and natural tugtupite, $Na_8[Be_2Al_2Si_8O_{24}](Cl,S)_{2-\delta}$, Phys. Chem. Minerals 39 (2012) 163–168.

[54] H.M. Rietveld, A profile refinement method for nuclear and magnetic structure, J. App. Cryst. 2 (1969) 65-71.

[55] V.Petricek, M. Dusek, L. Palatinus, Crystallographic Computing System JANA2006: General features, Z. Kristallogr. 229 (2014) 345-352.

[56] V. Jolivet, Y. Morizet, J. Hamon, et al. The influence of iodide on glass transition temperature of high-pressure nuclear waste glasses, J. Am. Ceramic Soc. 104 (2021) 1360–1369.

[57] D.S. Kim, D.K. Peeler, P. Hrma, Effect of crystallisation on the chemical durability of simulated nuclear waste glasses, Ceram. Bull. 61 (1995) 177–185.

[58] C.P. Rodriguez, J.S. McCloy, M.J. Schweiger, et al., Optical basicity and nepheline crystallization in high alumina glasses. US Department of Energy, Pacific Northwest National Laboratory (2011) 20184.

[59] D.B. Dingwell, S.L. Webb, Relaxation in silicate melts, Eur. J. Min. 2 (1990) 427–49.

[60] B. Vénague, L. Campayo, M.J. Toplis, et al., Role of alkalis on the incorporation of iodine in simple borosilicate glasses, J. Non-Cryst. Solids 576 (2022) 121278.

[61] M.R. Cicconi, E. Pili, L. Grousset, D.R. Neuville, The influence of glass composition on iodine solubility, Mat. Res. Soc. 4 (2019a) 971–979.

[62] M.R. Cicconi, E. Pili, L. Grousset, P. Florian, J.C. Bouillard, D. Vantelon, et al., Iodine solubility and speciation in glasses, Sci. Rep. 9 (2019b) 7758.

[63] F. Angeli, T. Charpentier, D. De Ligny, C. Cailleteau, Boron speciation in sodalime borosilicate glasses containing zirconium, J. Am. Ceram. Soc. 93 (2010) 2693-2704.

[64] J. Waser, E.D.Jr. McClanahan, The crystal structure of $NaPt_3O_4$, J. Chem. Phys. 19 (1951) 413-416.

[65] M.J. Buerger, G.E. Klein, G. Hamburger, Structure of Nepheline, Geol. Soc. Am. Bull. 57 (1946) 1182-1183.

[66] M.J. Buerger, G.E. Klein, G. Hamburger, The structure of nepheline, Am. Mineral. 32 (1947) 197.

[67] M.J. Buerger, G.E. Klein, G. Donnay, Determination of the crystal structure of nepheline, Am. Mineral. 39 (1954) 805-818.

[68] G. Diego Gatta, R.J. Angel, Elastic behavior and pressure-induced structural evolution of nepheline: Implications for the nature of the modulated superstructure, Am. Mineral. 92 (2007) 1446-1455.

[69] B. Beagley, C.M.B. Henderson, D. Taylor, The crystal structure of aluminosilicate-sodalites: X-ray diffraction studies and computer modelling, Min. Mag. 46 (1982) 459-464.

[70] A.V. Borhade, S.G. Wakchaure, A.G. Dholi, One pot synthesis and crystal structure of aluminosilicate mixed chloro-iodo sodalite, Indian J. Phys. 84 (2010) 133-141.

[71] S. Chong, J.A. Peterson, J. Nam, B.J. Riley, J. McCloy, Synthesis and characterization of iodosodalite, J. Am. Ceram. Soc. 100 (2016) 2273-2284.

[72] Z.D. Sharp, G.R. Helffrich, S.R. Bohlen, E.J. Essene, The stability of sodalite in the system $NaAlSiO_4$-NaCl, Geochim. Cosmochim. Acta. 53 (1989) 1943-1954.

[73] J.B. Schneider, D.M. Jenkins, Stability of sodalite relative to nepheline in NaCl-H_2O brines at 750°C: Implications for hydrothermal formation of sodalite, Can. Mineral. 58 (2020) 3-18.

Figure caption

Figure 1: Thermal history adopted in the experimental syntheses of the glass-ceramics under high-pressure conditions. The temperature history is divided into three parts: 1) melting (T_f) at ~1250°C for 1h, 2) nucleation (T_n) at ~550°C just above the glass transition temperature (T_g) determined by DSC at ~500°C and 3) crystallization (T_c) at ~790°C as determined by DSC measurements. The time for the T_n and T_c has been set to 24h. We used cooling and heating ramp of 15°C/min. At the end of the experiment, the sample is rapidly quenched.

Figure 2: DSC curves obtained for ambient pressure glasses: NH_1b and SoNH_1b; and I-bearing SoNH glasses: SoNH_I_2-0 and SoNH_I_2O_5-0. The reported T_g and T_n values were determined using the double tangent method and the crystallization peak position, respectively.

Figure 3: Elemental mapping obtained by high-resolution SEM on NH_I_2-2 and NH_I_2O_5-2 glass ceramic samples. The distribution of the element shows that most of the crystal are enriched with respect to iodine and correspond to iodosodalite (Is.). We also identified the presence of $NaPt_3O_4$ in NH_I_2O_5-2 and is a witness of a potential reaction in between the experimental charge and the Pt capsule walls. The crystal size does not exceed 5 μm.

Figure 4: Element mapping collected from S/TEM acquisition and obtained on NH_I_2-2 sample showing the coexistence of iodosodalite, nepheline and glass. The Ca map witnesses the presence of glass as Ca is absent from the structure of iodosodalite and nepheline.

Figure 5: X-ray Diffraction pattern obtained for NH_I_2-2 glass ceramic sample containing iodosodalite, nepheline and $NaPt_3O_4$. The residual suggests that the Rietveld refinement has been properly performed. We also added a β cage structure typical of the iodosodalite structure.

Figure 6: The bar plot shows the proportion of each crystalline phase determined in the glass ceramics from XRD treatment. Although, the refinement is incomplete for NH_I_2O_5-1

671 sample, there seems to be an increase in the iodosodalite proportion from I_2 to I_2O_5
672 experiments.
673

Table 1: Experimental conditions, temperature and time step for glass and glass ceramic syntheses, glass and matrix major element composition.

Sample	Pressure (GPa)	$I^{init.}$	T_g	T_f/t_f	T_n/t_n	T_c/t_c	Composition (mol.%)[a]					
							SiO_2	B_2O_3	Al_2O_3	CaO	Na_2O	I
Glass syntheses[b]							Glass					
NH_1b	0.0001	0	531	1300/2			39.9	19.7	10	8.6	21.8	
SoNH_1b	0.0001	0	510	1300/2			46.3	13.6	11.0	5.0	24.2	
NH_I_2-0	1.0	11.6		1300/3			41.5	20.7	10.5	6.9	19.7	0.7
NH_I_2O_5-0	1.0	10.6		1300/3			43.6	20.7	11.1	6.9	16.2	1.5
SoNH_I_2-0	1.0	9.6	510	1300/10			48.6	13.6	11.3	5.3	20.5	0.6
SoNH_I_2O_5-0	1.0	8.7	513	1300/10			50.3	13.6	11.7	5.1	18.1	1.2
Glass ceramic syntheses[b]							Matrix: Glass + nepheline					
NH_I_2-1	1.0	4.6		1300/1	594/24	813/24	43.4	19.7	9.4	8.6	18	0.3
NH_I_2O_5-1	1.0	4.0		1300/1	594/24	813/24	42.8	19.7	9.1	8.4	19.1	0.5
NH_I_2-2	1.0	10.2		1300/1	594/24	813/24	43.3	19.7	9.7	8.2	19	0.1
NH_I_2O_5-2	1.0	9.9		1300/1	594/24	813/24	45.1	19.7	10.4	7.7	16.9	0.3
SoNH_I_2-1	1.0	10.1		1300/2	560/24	785/24	48.9	14.4	8.1	8.1	20.3	0.8
SoNH_I_2O_5-1	1.0	11.5		1300/2	560/24	785/24	48.1	14.6	13.0	4.0	19.9	0.4
SoNH_I_2-3	1.5	11.1		1200/1	560/24	790/24	48.9	14.9	9.8	5.5	20.3	0.5
SoNH_I_2O_5-3	1.5	9.4		1200/1	560/24	790/24	48.6	15.3	10.0	5.4	20.4	0.4

[a]The composition of the of the matrix is reported in mol.%. The error on each oxide is on the order of ±0.5 mol.% based on the replicated measurements from SEM EDS. For I, the error is slightly lower at ±0.2 mol.%. It should be pointed out that the reported compositions are for pure glass and for glass+nepheline for glass and glass-ceramic syntheses, respectively. This is due to the fact that the nepheline cannot be distinguished from the glass in the glass-ceramic matrix.

[b]The experimental conditions read as follow. For glass, there is a one-step synthesis with melting at high-temperature (T_f). For glass-ceramics, there is a three-step synthesis protocol with melting (T_f), nucleation (T_n) and crystal growth (T_c). The time for T_n and T_c has been set to 24h. The whole protocol was performed under high-pressure conditions.

Table 2: X-ray Diffraction and Rietveld refinement results, cell parameters, phase proportion and iodine concentration in iodosodalite.

Crystalline phase	Cell parameters[a]						Cell volume (Å^3)	Space group	Proportion (wt.%)	wRp (%)	Mol.% I[b]
	a (Å)	b	c	α (°)	β	γ					
Iodo 1bar[c]											
Iodosodalite	9.0295(2)	9.0295	9.0295	90	90	90	736.2	I-43m	100	12.82	
NH_I_2-1											
Iodosodalite	9.007(1)	9.007	9.007	90	90	90	730.8	I-43m	52.8±1.7	1.98	10.5
Nepheline	9.946(3)	9.946	8.326(4)	90	90	120	713.3	P63	47.2±1.6		
NH_I_2-2											
Iodosodalite	9.008(2)	9.008	9.008	90	90	90	731.1	I-43m	59.1±1.4		9.3
Nepheline	9.949(3)	9.949	8.331(4)	90	90	120	714.1	P63	39.0±1.4	2.02	
$NaPt_3O_4$	5.680(3)	5.680	5.680	90	90	90	183.3	Pm-3n	1.9±0.2		
SoNH_I_2-1											
Nepheline	9.937(8)	9.937	8.316(9)	90	90	120	711.1	P63	73.6±1.7		
Iodosodalite	9.007(7)	9.007	9.007	90	90	90	730.7	I-43m	24.5±1.7	2.89	10.4
$NaPt_3O_4$	5.692(4)	5.692	5.692	90	90	90	184.4	Pm-3n	1.9±0.2		
SoNH_I_2-3											
Nepheline	9.921(6)	9.9212	8.299(6)	90	90	120	707.5	P63	91.7±0.9	4.06	
Iodosodalite	8.999(9)	8.999	8.999	90	90	90	728.9	I-43m	8.3±0.9		13.3
NH_I_2O_5-1[d]											
Iodosodalite	9.0113(5)	9.0113	9.0113	90	90	90	731.7	I-43m	54.0±0.2		14.1
Nepheline	9.947(8)	9.947	8.327(10)	90	90	120	713.6	P63	29.0±0.2	2.35	
$NaPt_3O_4$	5.680(1)	5.680	5.680	90	90	90	183.3	Pm-3n	16.0±1.5		

[a] The lattice parameters of the different crystalline phases has been determined using Rietveld refinement of the structure with JANA2020©. The error bars on each parameter is calculated with the Berar's factor and the normalized error obtained on the fit. For the different phases, we used standard crystalline structure collected from the Crystallographic Open Database. The reliability parameter (wRp) corresponds to a satisfaction parameter.

[b] The mol.% I corresponds to the I concentration determined from SEM EDS measurements based on several replicated measurements.

[c] The XRD acquisition for this sample was carried out with a Bragg-Brentano geometry, whereas the other samples were characterized with Debye-Scherrer geometry using capillary.

[d] For NH_I_2O_5-1 and for I_2O_5 glass ceramic samples, more generally, we did not manage to obtain a satisfying Rietveld refinement. Therefore, the error on the phase proportions is probably large and the cell parameters are likely to be accompanied with a large error.

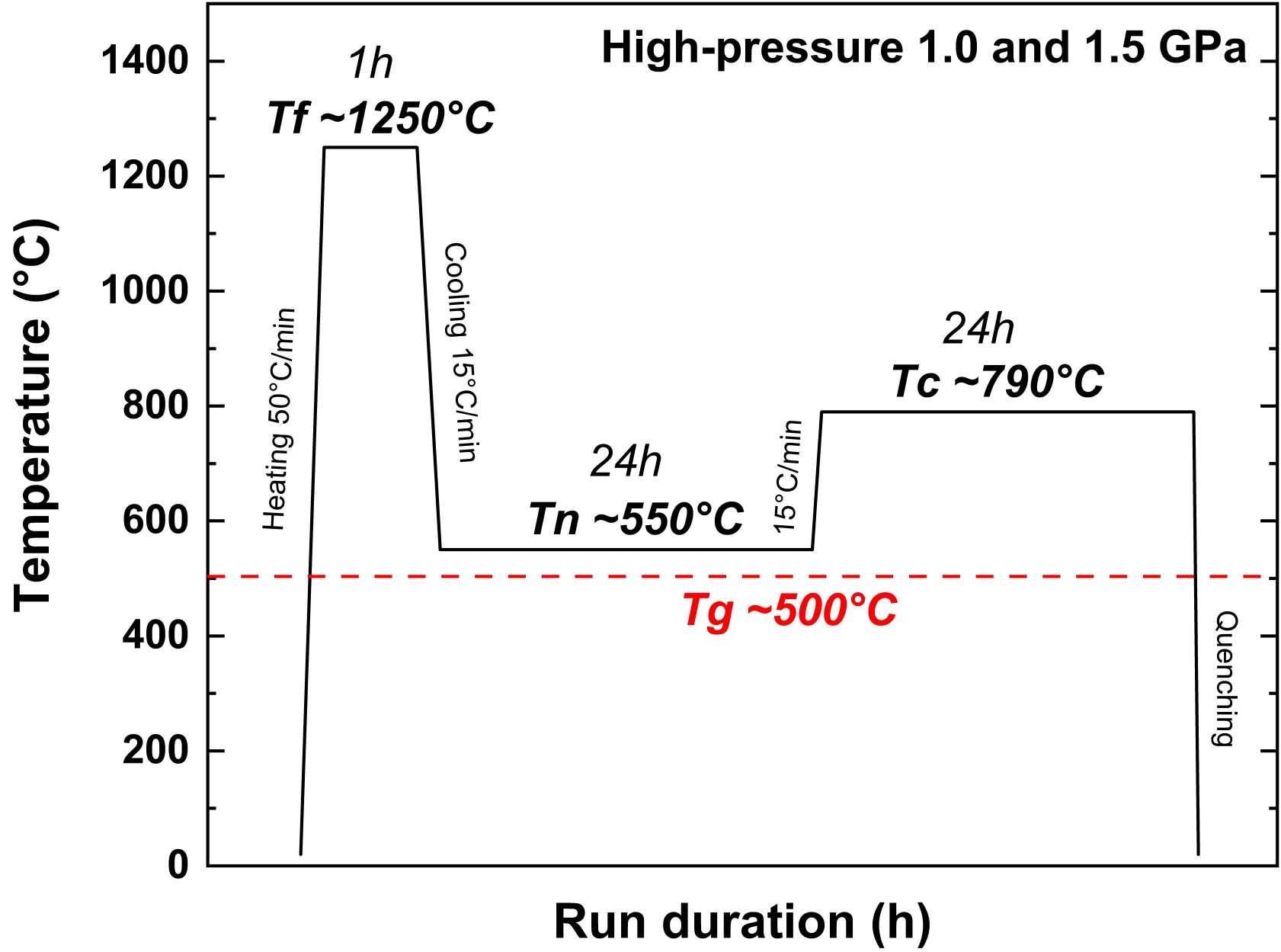
High-pressure 1.0 and 1.5 GPa
1h
Tf ~1250°C
Heating 50°C/min
Cooling 15°C/min
24h
Tn ~550°C
15°C/min
24h
Tc ~790°C
Tg ~500°C
Quenching
Temperature (°C)
Run duration (h)
0
200
400
600
800
1000
1200
1400

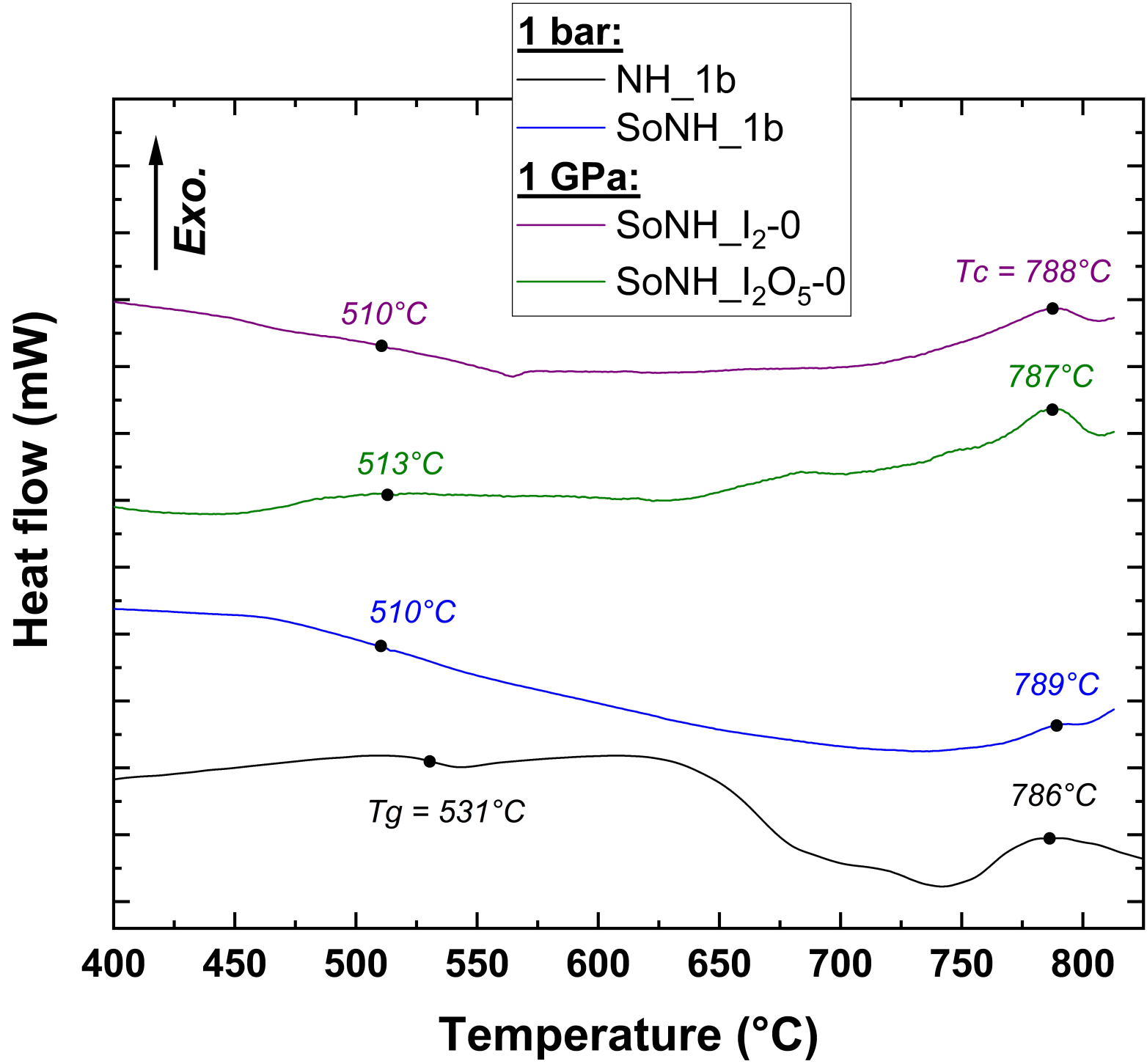
1 bar:
NH_1b
SoNH_1b
1 GPa:
SoNH_I2-0
SoNH_I2O5-0
Exo.
Tc = 788°C
510°C
787°C
513°C
510°C
789°C
Tg = 531°C
786°C
Heat flow (mW)
400
450
500
550
600
650
700
750
800
Temperature (°C)

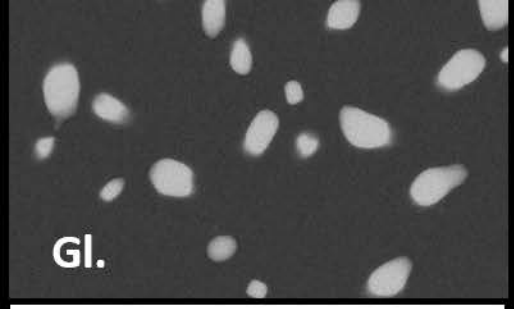

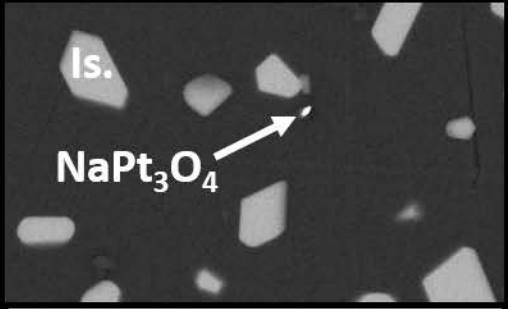

NH_I_2-2: 1.0 GPa + I_2

NH_I_2O_5-2: 1.0 GPa + I_2O_5

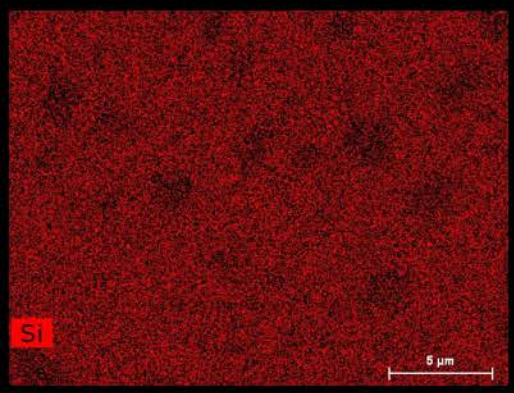

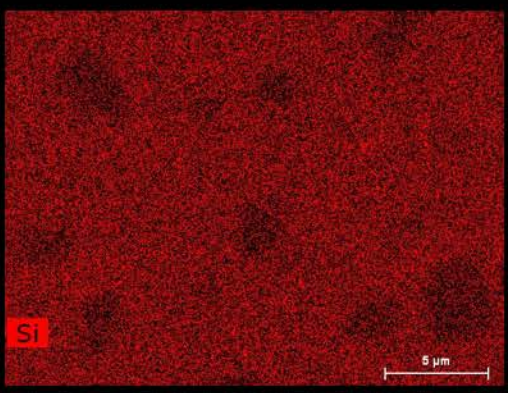

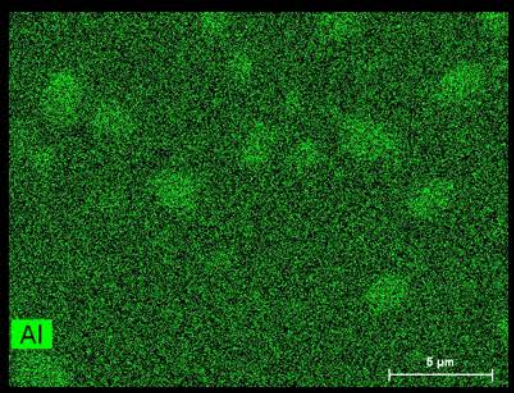

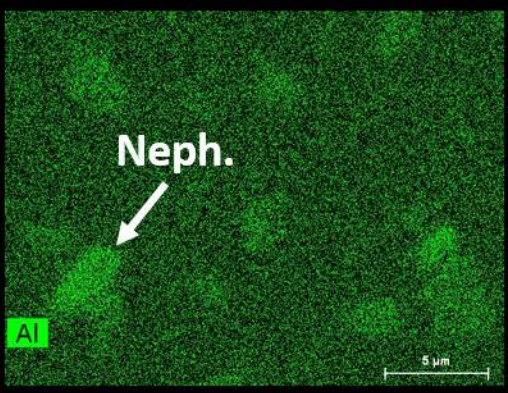

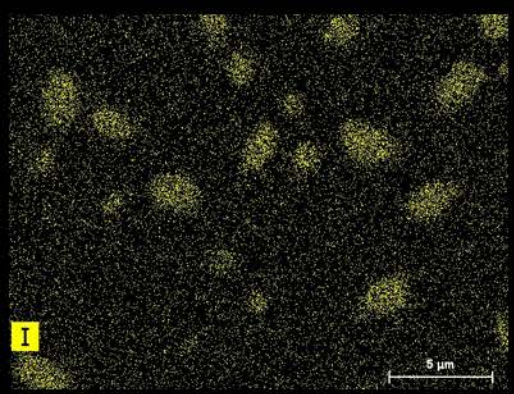

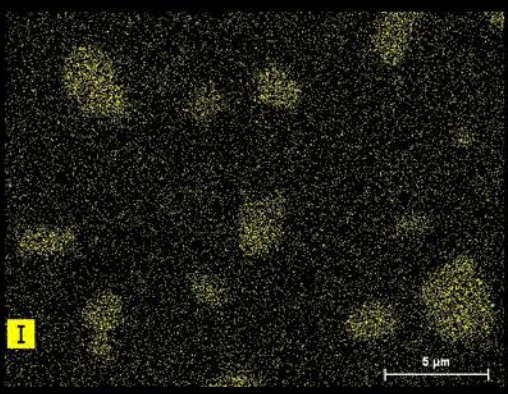

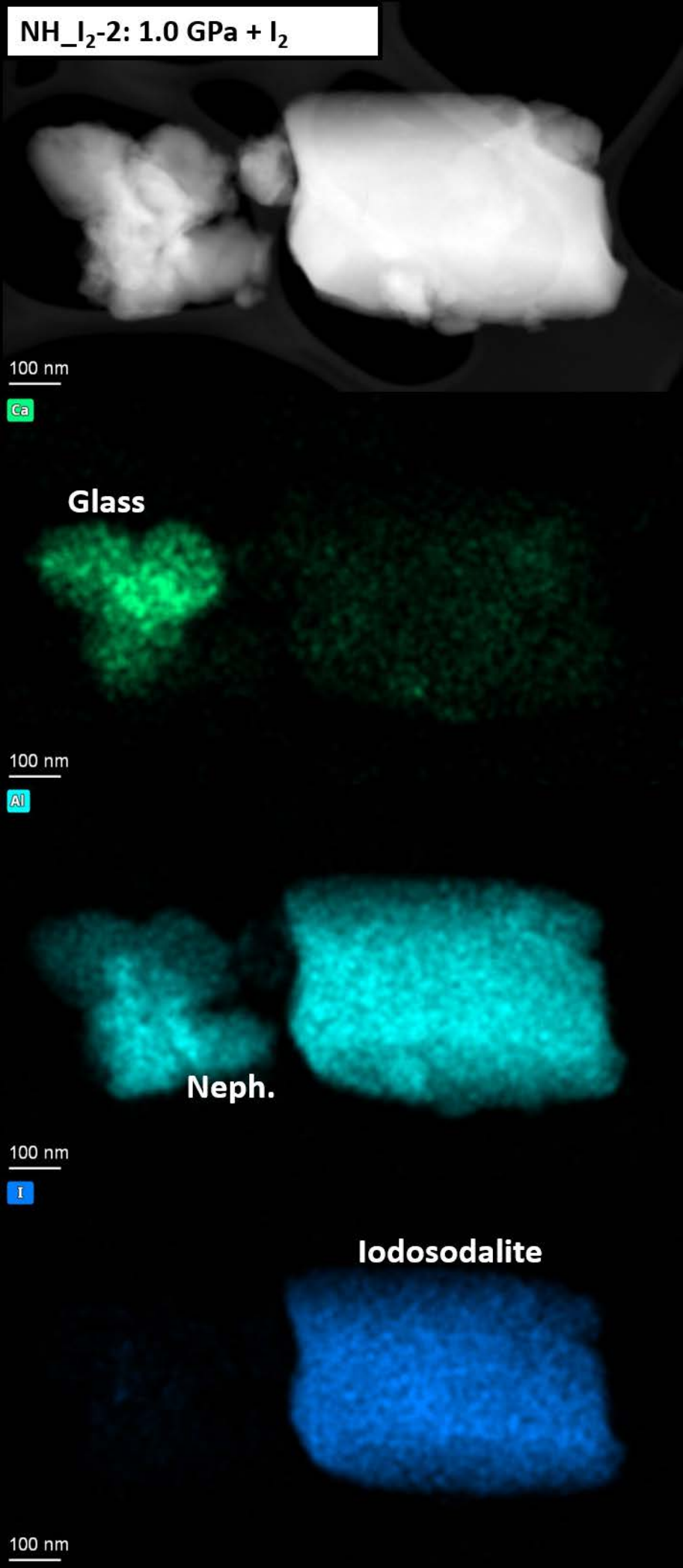
NH_I2-2: 1.0 GPa + I2
100 nm
Ca
Glass
100 nm
Al
Neph.
100 nm
I
Iodosodalite
100 nm

NH_I$_2$-2 *1 GPa - 24h nucleation + 24h growth*

Observed
Simulated
Residual
Iodosodalite
Nepheline
$NaPt_3O_4$

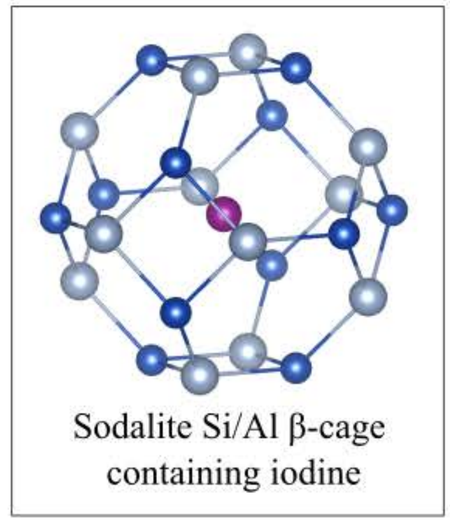

Sodalite Si/Al β-cage containing iodine

Amorphous bump

Intensity (a.u.)

20 30 40 50 60 70

2θ (Degrees)

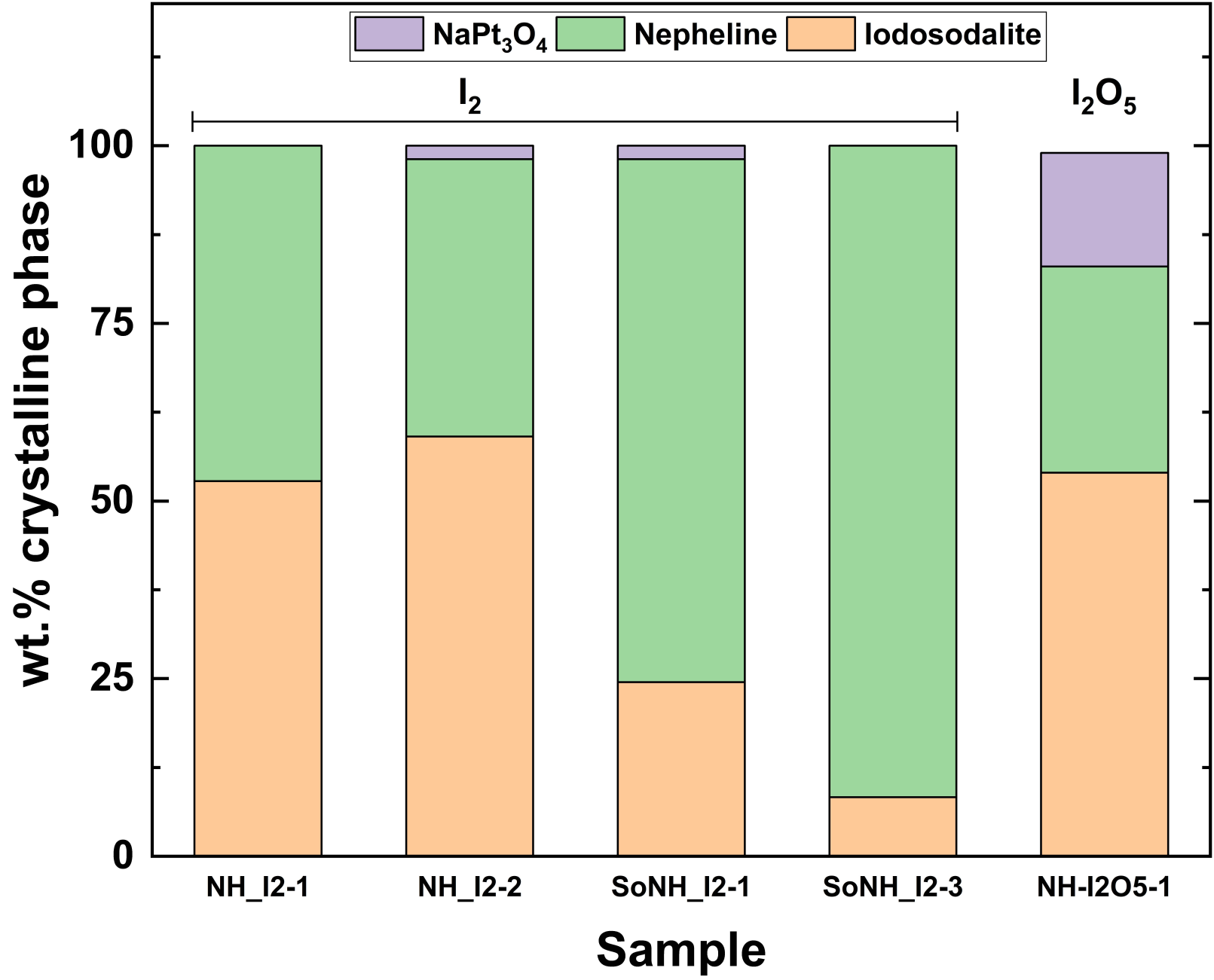
NaPt3O4
Nepheline
Iodosodalite
I2
I2O5
100
75
50
25
0
wt.% crystalline phase
NH_I2-1
NH_I2-2
SoNH_I2-1
SoNH_I2-3
NH-I2O5-1
Sample

SUPPLEMENTARY MATERIAL: HIGH-PRESSURE REAL GLASS-CERAMICS FOR IODINE NUCLEAR WASTE IMMOBILIZATION: PRELIMINARY EXPERIMENTAL RESULTS

1. X-ray Diffraction patterns

We acquired X-ray diffraction patterns for each of the glass ceramics sample and the iodosodalite synthesized at 1 bar pressure. The diffractograms are shown in the Figure S1. The peaks for each crystalline phase are also shown. We do not show the Rietveld refinement; however, refinements are available on demand for I_2 loaded samples.

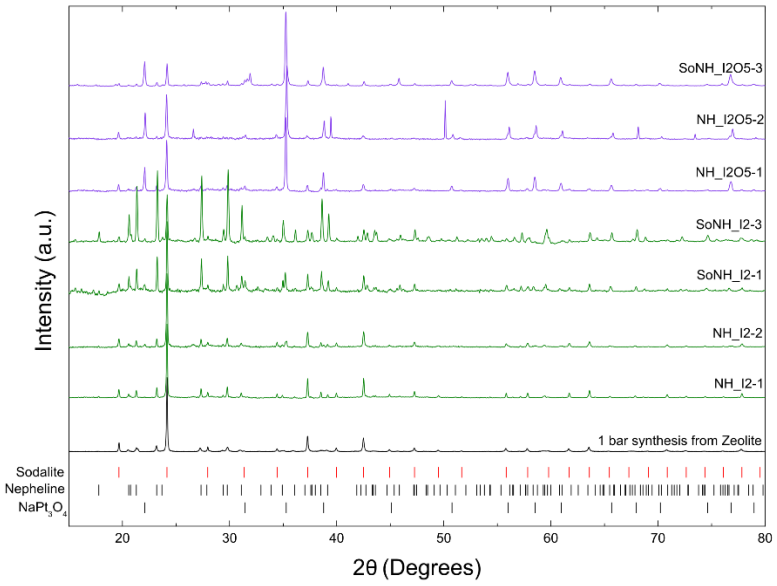

Figure S1: X-ray Diffraction patterns obtained on the glass ceramics in the present study.

2. Evidence for Pt capsule walls and inside experimental charge chemical reaction

For the SoNH_I_2O_5-0 and SoNH_I_2-0 glass syntheses (see Table 1) conducted at 1.0 GPa and 1300°C for 10h, we have analyzed the Pt container walls to evaluate the potential reaction between the inside experimental charge and the walls. The measurements were performed on a Wavelength Dispersive Spectroscopy Scanning Electron Microscope (WDS SEM) at the

IMN Jean Rouxel Polytech Nantes. The acquisitions are carried out on a Zeiss Merlin equipped with a WDS probe. We used a 15 kV acceleration current and the samples were mounted in an epoxy plug and analyzed without carbon coating.

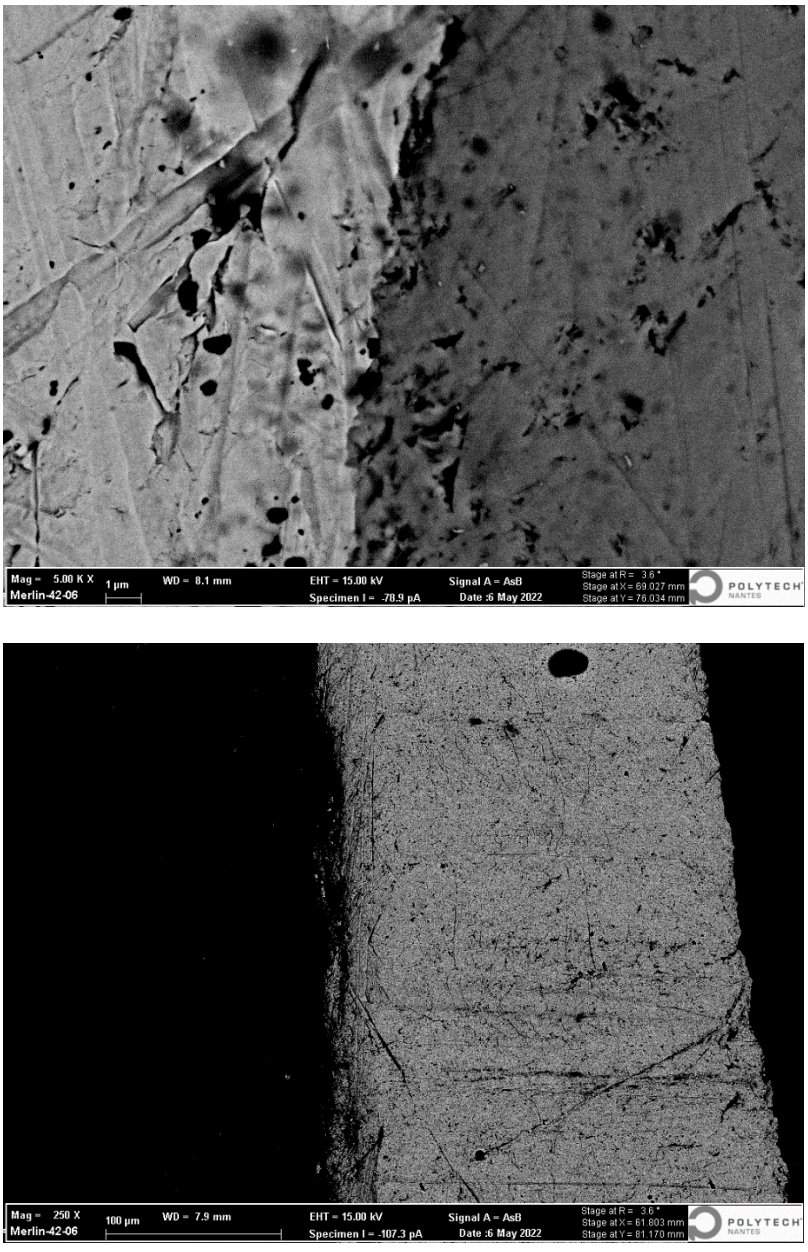

Figure S2: Backscattered Electron Microscope image obtained on the Pt capsule walls for SoNH_I_2-0 (Bottom) and SoNH_I_2O_5-0 (Top) samples. The images are shown at different magnification. We observe a contrast in color for SoNH_I_2O_5-0 in the Pt walls indicating a change in the composition of the walls. The element concentration (see Table S1) shows an increase in the O concentration in the inside of the Pt capsule wall.

The images are shown in Figure S2 for SoNH_I_2O_5-0 and SoNH_I_2-0 at different magnifications and showing a portion of the Pt capsule walls. For SoNH_I_2O_5-0, we clearly observe that there is a contrast in the Pt wall between a brighter color on the left and a darker color on the right hand side. This is explained by a difference in the chemical composition. This difference in chemical composition within the capsule wall is not visible for the SoNH_I_2-0 sample suggesting a homogeneous composition of the Pt walls. We have quantified the element in each part of both SoNH_I_2-0 and SoNH_I_2O_5-0 samples. The results are provided in the following Table S1.

	Na (mol.%)	Ca	O	Pt
	SoNH_I2O5-0			
Outer Pt wall	0	0	11.2	88.8
Inner Pt wall	6.5	1.9	37.7	53.9
	SoNH_I2-0			
Pt wall	0	0	6.3	93.7

Table S1: Element concentrations in mol.% determined from WDS analyses in the Pt walls for SoNH_I_2-0 and SoNH_I_2O_5-0. The error on the reported concentrations is on the order of ±10% in relative to the value.

For SoNH_I_2-0, the capsule wall is mostly represented by Pt at 94 mol.% and is slightly enriched in O at 6 mol.%. We find roughly the same composition for the outer Pt wall for SoNH_I_2O_5-0 sample. For the inner Pt wall of SoNH_I_2O_5-0 we clearly observe that there is a strong chemical reaction with the Pt alloying with the available O in the experimental charge but also Ca and Na. the O concentration measured is as high as 38 mol.%. Such a high O concentration is explained by the presence of excess O in the experimental charge coming from the dissociation of I_2O_5 into I_2 and O_2 above 350°C. The Pt-O alloying in the I_2O_5 experiments could explain the presence of identified $NaPt_3O_4$ observed from XRD (see Table 2).